8-20-2003

A Model of Zebra Emission in Solar Type IV Radio Bursts

J. LaBelle
Dartmouth College

R. A. Treumann
Dartmouth College

P. H. Yoon
University of Maryland at College Park

M. Karlicky
Czech Academy of Sciences

The Astrophysical Journal, 593:1195–1207, 2003 August 20

A MODEL OF ZEBRA EMISSION IN SOLAR TYPE IV RADIO BURSTS

J. LaBelle,[1] R. A. Treumann,[2,1] P. H. Yoon,[3] and M. Karlicky[4]

Received 2003 March 4; accepted 2003 May 6

ABSTRACT

Solar type IV radio bursts present a theoretical challenge because they are composed of both continuum emission and fine structures. The latter include "zebra bursts," which appear as harmonically spaced multiplets that shift in frequency with time. Similarities between these features and terrestrial auroral emissions suggest a new model to explain zebra-structured type IV emissions. In this model, the basic generation mechanism is identical with that proposed by Winglee and Dulk: mode conversion of Z-mode waves generated by the cyclotron maser mechanism under the condition $f_{uh} = Nf_{ce}$, with N an integer; however, we propose a twist on this model whereby the "zebra bursts" do not arise from multiple N-values. Rather, the presence of localized density irregularities within the type IV source region leads to trapping of the upper hybrid Z-mode waves in density enhancements, which results in a discrete spectrum of upper hybrid modes with nearly constant frequency spacing. The number m of quasi-harmonics is limited by the trapping (quantization) conditions. The problem is described by an equivalent Schrödinger equation for the trapped mode, which is solved for an (idealized) cylindrical square density irregularity. In this model, the eigenfrequency spacing matches the observed type IV frequency spacings for less than 10% density enhancements with individual scale sizes of 30–1000 thermal electron gyroradii, corresponding to 1–100 m scales in coronal loops. To produce the observed emitted power for a reasonable (<1%) efficiency requires a large number of such individual microscopic sources occurring over a portion of a magnetic type IV loop at a restricted altitude within which the magnetic field and density are approximately constant. The loop plasma in the zebra emission source is thus highly turbulent in the sense that it contains a large number of density fluctuations. In this case transition radiation can effectively contribute to the radiation background and may also provide the wave power required in the upper hybrid range for generating zebra emissions.

Subject heading: Sun: radio radiation

1. INTRODUCTION

Type IV solar radio emissions are related to the injection of large fluxes of mildly energetic electrons into a coronal loop. These trapped electrons gyrate and bounce in the loop magnetic field. The resulting incoherent radio emission in the decimetric to decametric wavelength range maps out the location and motion of the loop in the solar corona. The nonthermal type IV emission from the gyrating particles is complex, consisting of both a structureless continuum and a number of fine structures referred to as pulsations, fibers, spaghetti, zebra bursts, and many other descriptions. Among the most remarkable of the fine structures is the zebra emission, named after its zebra stripe appearance on a dynamic spectrogram. It occurs at both metric and decimetric wavelengths. It was first reported by Slottje (1972) and observed extensively in the metric wavelengths (Slottje 1981; Bernold 1980; Chernov 1996; Kuipers, van der Post, & Slottje 1981; and others) and also at decimetric wavelengths (e.g., Jiřička et al. 2001; Ledenev et al. 2001). The zebra emission consists of a series of spectral bands. The spacing between the bands is approximately constant with slight systematic variation, which in many cases is hard to resolve because of the limited resolution of the radio receivers. The different bands move as an entity across the spectrum, in many cases undulating around a quasi-stationary spectral position. Usually the number of such zebra bands within one zebra burst is large (>5–8, sometimes even exceeding 20). Observationally it remains unclear whether zebras are emission or absorption lines on an otherwise slowly varying continuous spectral type IV background, although observations of zebra bands when the type IV background is weak suggest that zebras are quasi-harmonic emission lines, in contrast to other fine structures such as "fiber emissions" (see, e.g., Treumann, Güdel, & Benz 1990), which consist of emissions and absorption in close connection. Frequency spacings are on the order of 1–18 MHz for metric zebras (e.g., histogram in Slottje 1981) and on the order of tens of megahertz for decimetric zebras (e.g., Jiřička et al. 2001).

Since the loss cone feature of trapped electrons in a coronal loop can naturally stimulate both electrostatic electron Bernstein waves at harmonics Nf_{ce} of the local electron cyclotron frequency f_{ce}, as well as electrostatic upper hybrid $f \sim f_{uh}$ waves ($f_{uh}^2 = f_{ce}^2 + f_{pe}^2$), early theories proposed that wave-wave interaction between these modes leads to radiating modes with frequency spacings approximately equal to the local f_{ce} in the source (Rosenberg 1972; Chiuderi, Giachetti, & Rosenberg 1973). However, these theories do not easily account for features of zebra bursts such as the rapid changes in frequency or the occasional splitting of

[1] Department of Physics and Astronomy, 6127 Wilder Laboratory, Dartmouth College, Hanover, NH 03755-3528; jlabelle@einstein, dartmouth.edu.

[2] Centre for Interdisciplinary Plasma Science, Max Planck Institute for extraterrestrial Physics, Giessenbachstrasse Postfach 1312, Garching D-85741, Germany; tre@mpe.mpg.de.

[3] Institute for Physical Science and Technology, University of Maryland, College Park, MD 20742.

[4] Astronomical Institute, Academy of Sciences, Dr. Frice 1, Ondřejov CZ-251 65, Czech Republic.

lines. Furthermore, they require too low a magnetic field to account for the spacing of the bands. Alternative theories based on whistler wave packets (Chernov 1990, 1996) or whistler solitons (Treumann & Bernold 1981) propagating across or along the region where the trapped electron distributions emit type IV continuum or inertial kinetic Alfvén waves for type IV fine structures (Treumann et al. 1990) have also been proposed. These theories have difficulty explaining why a large number of zebra bands occur simultaneously and why the emissions at widely different frequencies across the spectrum shift frequency in tandem almost simultaneously. Such simultaneous occurrence and coordinated motion suggests that the emissions are confined to a narrow location in physical space. In addition, whistler soliton formation in solar magnetic loops of high field strength is improbable as it requires substantial bending of the magnetic field lines, which under the conditions usually encountered there $\beta \ll 1$ is difficult to justify. Another possibility is that the emissions result from transformation of strongly localized electrostatic ion cyclotron waves at the base of the corona, which are known to occur when field-aligned currents flow or ion beams propagate across the magnetic field, but this model requires that the magnetic field strength in the source region, inferred from the frequency spacing of the resulting emissions, is unreasonably high, on the order of more than 10^3 G for 1 MHz spacing as observed for metric type IV zebra emissions or on the order of more than 10^4 G for 10 MHz spacing as observed for decimetric zebra emissions. Other theories have been proposed involving scattering of the high-frequency waves on nonlinear sound waves (e.g., Fomichev & Fainshtein 1981).

The most successful theories involve the upper hybrid double-resonance condition, which occurs in an overdense plasma when $f_{uh} = Nf_{ce}$, with N an integer. Theories of this kind have been presented by Zheleznyakov & Zlotnik (1975) and Winglee & Dulk (1986). In both cases, the generated mode is electrostatic, and radiation requires mode conversion. Winglee & Dulk (1986) point out that in the presence of the loss cone distribution function implied by the trapping of electrons in the coronal loop the cyclotron maser mechanism results in large growth rates for Z-mode waves for the conditions $f_{pe}/f_{ce} = 1.7$, $f_{pe}/f_{ce} = 2.8$, etc., corresponding to $f_{uh} = Nf_{ce}$. Inhomogeneity plays a key role in this model: if the dominant inhomogeneity is the gradient in plasma density, then the double-resonance condition acting over a region of space will produce N nonoverlapping harmonics and a zebra-type emission results; on the other hand, if the dominant inhomogeneity is the gradient in magnetic field, the harmonics generated by the double-resonance condition overlap, leading to continuum emission. In this way, Winglee & Dulk (1986) explain with one mechanism a range of type IV emission characteristics. This theory requires a relatively low magnetic field and high density to obtain a large number N of harmonics, because each observed harmonic represents a separate double-resonance condition. The emissions come from spatially separated locations. Though not in contradiction to observation, this runs contrary to the inference of a compact source size suggested by the tendency of a wide range of bands to change frequency in tandem almost simultaneously. It requires that the variations of the emission properties along a loop have a high degree of coherence.

In this paper, we propose a variant of the model of Winglee & Dulk (1986). We adopt their excitation mechanism of upper hybrid waves being the electrostatic high-frequency branch of the electromagnetic Z-mode. As in their case, the Z-mode is assumed to be generated via the cyclotron maser mechanism under the condition of an overdense plasma with plasma frequency $f_{pe} > f_{ce}$ exceeding the electron cyclotron frequency, while the emitted radiation is generated at the double resonance $f_{uh} = Nf_{ce}$. Also, as in their case, further unidentified mode conversion of the resulting electrostatic upper hybrid waves is required to obtain escaping free-space electromagnetic radiation mostly in the X-mode. The difference with their model lies in that the individual zebra components do not correspond to different integers N in the double-resonance condition. Rather, all the emissions correspond to the same value of N, most likely to small $N = 2$ or 3, where cyclotron damping is negligible, as occurs commonly, for example, in the generation of auroral roar emissions in the terrestrial auroral ionosphere (see, e.g., Shepherd, LaBelle, & Trimpi 1998). The formation of the zebra stripes occurs because localized density enhancements trap the upper hybrid waves and impose a discrete frequency spectrum on them. In this model, all the zebra bands are generated in one small volume. This is suggested by the simultaneous rapid variations in the frequencies of the zebra components. Imaging observations indicate a much broader source, a fact to which we will return later.

The theory put forth in this paper explains only the source of the frequency-time structure of the radiation. It does not include effects of radiation transport such as propagation, absorption, and reradiation, although these undoubtedly exert significant effects, even in the case of an optically thin medium. Below, we briefly consider examples of experimental data. We then compare the results to calculations of the frequency spacing inferred from the model on the basis of parameters of the generation region.

2. OBSERVATIONS

Figure 1 shows spectra of a decimetric type IV solar radio burst detected at Ondřejov Observatory in the Czech Republic on 1998 May 2. The dynamic spectrogram Figure 1 (*left*) covers 1.2–1.6 GHz, and white represents high power spectral densities, while dark represents low intensity. The zebra pattern is evident, with more than six bands shifting in frequency simultaneously on timescales less than 1 s. Figure 1 (*right*) shows a single average spectrum, showing that the frequency spacing between zebra bands is approximately 30 MHz in this example. Furthermore, the spacing between the bands is approximately constant over the frequency range covered by six to eight bands, and the width of each band is of the same order as the spacing between them. There is also evidence in both panels for a continuum component in addition to the zebra bands. In this example the zebras appear to most likely represent emission bands superposed on a weak continuum background type IV emission. In some cases, decimetric zebra structures occur in two branches roughly harmonically related, as in observations of Ledenev et al. (2001) showing simultaneous zebra features at 1.0–1.4 and 2–3 GHz (their Fig. 2).

Figure 2, taken from Chernov (1996), shows an example of a metric type IV zebra emission recorded at the IZMIRAN Observatory on 1989 March 12. Contrary to Figure 1, dark represents high power spectral densities, while white represents low intensity. In this example the

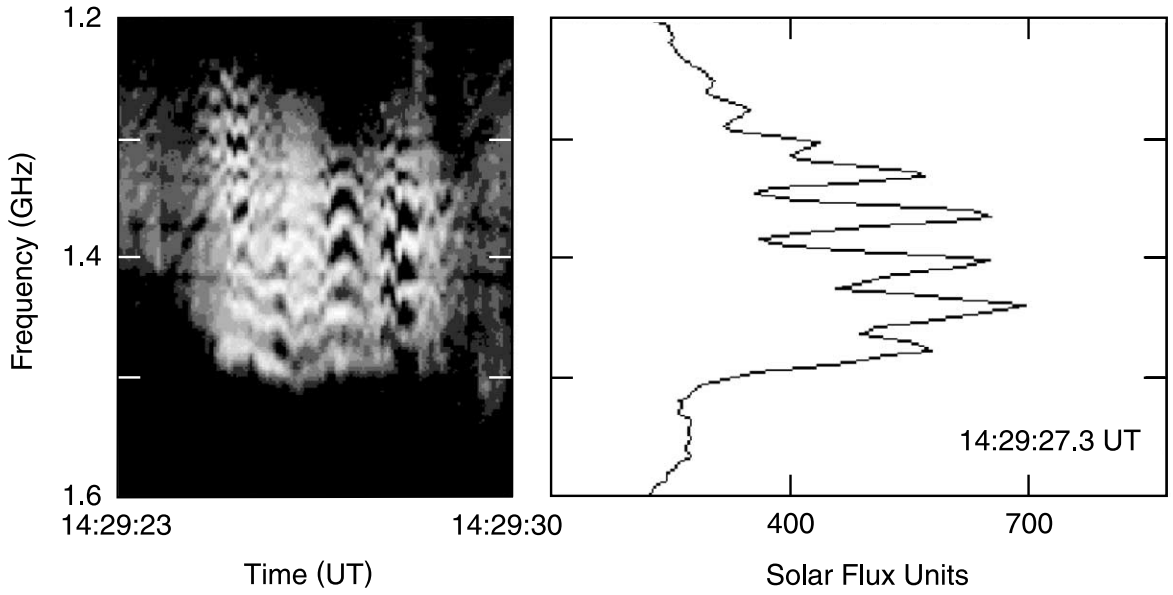

FIG. 1.—Example of decimetric solar type IV emission showing zebra structure, recorded at Ondřejov Observatory, Czech Republic, 1998 May 2

spacing between the zebra bands is of the order of 5 MHz and is roughly constant at any given time across the more than eight observed bands. The bands move up and down in frequency by tens of megahertz on timescales of seconds. All the observed bands shift in frequency simultaneously. As in the decimetric case, metric zebra emissions also show evidence for a mixture of continuum radiation, zebra structures, and other fine structures. The frequency spacing observed in the metric zebras can sometimes be as narrow as 1 MHz (Slottje 1981).

Zebra emissions strikingly resemble the fine structure of auroral roar emissions originating in the F-region of the Earth's auroral ionosphere and observed at ground level (LaBelle et al. 1995; Shepherd et al. 1998). These terrestrial auroral emissions occur at approximately 3 and 4.5 MHz and have bandwidths of up to a few hundred kilohertz. As with type IV, the emissions show a complicated mix of continuum and fine structures, including many fiber-like and spaghetti-like features superposed on a continuous background. At times, multiple discrete frequencies occur separated by a few kilohertz, which shift in frequency simultaneously on subsecond timescales (for example, Fig. 4 of Shepherd et al. 1998). These features, called "multiplets" by Shepherd et al. (1998), strongly resemble zebra emissions. As with decimetric type IV, auroral roars are occasionally observed simultaneously at widely spaced frequencies, near 3 and 4.5 MHz versus 1.0–1.4 and 2–3 GHz in the decimetric type IV event studied by Ledenev et al. (2001). Auroral roar has been attributed to cyclotron maser–generated Z-modes at the double resonance (e.g., Yoon, Weatherwax, & Rosenberg 1998; review by LaBelle & Treumann 2002, and references therein), and recently Yoon, Weatherwax, & LaBelle (2000) reported a theory to explain the multiplet structure, inspired by work of McAdams, Ergun, & LaBelle (2000) explaining similar frequency fine structures in rocket observations of auroral Langmuir upper hybrid waves. These observations and theories of auroral roar emissions inspire the model of type IV put forth below, which is a variant of the generation mechanism put forth by Winglee & Dulk (1986).

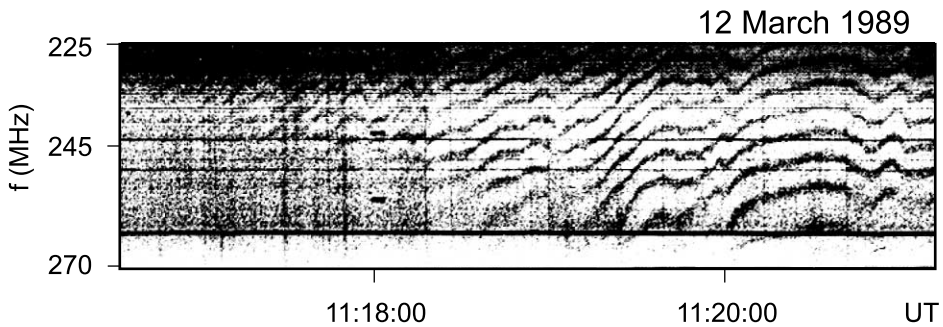

FIG. 2.—Example of metric solar type IV emission showing zebra structure, recorded at IZMIRAN Observatory, 1989 March 12. Note that in comparison with Fig. 1 the gray scale has been inverted here. Now the zebra emissions are the dark lines.

3. THEORETICAL MODEL

Following the McAdams et al. (2000) explanation for Langmuir wave fine structure observed with sounding rockets and the Yoon et al. (2000) explanation for fine structure in terrestrial auroral roar emissions, we put forth that the solar type IV fine structure may be interpreted by a similar mechanism in terms of upper hybrid wave trapping. The upper hybrid waves may have been excited in solar magnetic loops by the energetic trapped electron distribution injected into the loop during type IV radio bursts. As mentioned above, the most probable excitation mechanism is the one proposed by Winglee & Dulk (1986) in which the waves are generated by the electron cyclotron maser instability in an overdense plasma $(f_{pe}/f_{ce})^2 > 1$ at the double-resonance condition $f_{uh} = Nf_{ce}$. This mechanism works in the (electromagnetic) Z-mode below the upper hybrid frequency. Close to f_{uh} the Z-mode becomes electrostatic, which is favorable for wave trapping in density inhomogeneities. Whenever the upper hybrid waves become trapped in regions of appropriate-scale cylindrical field-aligned density striations, they will evolve into a trapped mode exhibiting a discrete wavenumber spectrum and hence also a discrete frequency spectrum of a limited number of distinct quasi-harmonic trapped eigenmodes the frequency spacing of which is determined by the nature of the density variation.

Below we show that to be effective in upper hybrid wave trapping these density variations must necessarily be enhancements of density over background. On conversion to an escaping radiating mode, these modes most probably retain the discrete frequency spectrum imposed by the trapping conditions. The result is a complicated mix of radiation features: at times when the density structure in the source region is appropriate, zebra emissions may dominate, with frequency variations corresponding to variations in the density structure. At other times, wave trapping may be inefficient or nonexistent, and the resulting radiation will be dominated by the type IV continuum radiation. In the case of the appearance of zebra bands, the bands must originate in a rather large number of physically small density enhancements (the wave-trapping structures) of similar characteristics, which may be packed within a volume much smaller than a coronal loop but still of macroscopic size for producing an observable modulation of radio wave emissivity. Thus, this model of zebra emissions involves generation of all the zebra bands within a relatively small volume, as is suggested by the observations discussed above.

We proceed to calculate the eigenfrequencies of the trapped Z-modes within a single electron density enhancement by using a simple "waterbag" model for the density enhancement. This simple model is analogous to applying the Schrödinger equation to a square-well potential in quantum mechanics. It gives an analytical expression for the energy levels that is easily evaluated numerically to give an estimate of the eigenfrequency spacing. By using plasma and magnetic field parameters corresponding to type IV magnetic loops in the solar corona and matching the resulting eigenfrequencies to the observed type IV frequency spacings, the model predicts the size of the trapping density irregularity at the source. The frequency spacing depends naturally on the shape of the density irregularity. The estimate based on the square irregularity thus provides only a guide to the range of source sizes that can occur in the case of real density irregularities.

The wave electric field associated with the upper hybrid mode in a cylindrical plasma column with radial density variation is governed by the equation

$$\frac{1}{r}\frac{d}{dr}\left(r\frac{dE}{dr}\right)+\frac{1}{r^2}\frac{d^2E}{d\phi^2}+k_\perp^2(r)E=0\,. \tag{1}$$

The dispersion relation of the upper hybrid Z-mode waves implies

$$k_\perp^2(r)=\frac{2}{\rho_e^2}\frac{\Omega_{ce}^2}{\omega_{pe}^2(r)}\left[\frac{\omega_{pe}^2(r)+\Omega_{ce}^2}{\omega^2}-1\right]. \tag{2}$$

Note that this dispersion relation includes the electron temperature through the electron gyroradius $\rho_e = (2k_BT_e/m\Omega_{ce}^2)^{1/2}$ and therefore describes upper hybrid Z-mode waves propagating in a hot electron plasma of temperature T_e. Cold plasma theory is irrelevant to our calculation, since in that limit the Z-modes degenerate to a pure oscillation, inhibiting wave trapping. Further kinetic effects are not considered here; such effects are important for determining the growth rate of the Z-mode (see, for example, Winglee & Dulk 1986), but they have higher order effects only on the real part of the dispersion relation; therefore we neglect them here. The objective of this calculation is to obtain an estimate of required characteristics of the trapping density enhancements. To this end, we use the simplest relevant theoretical framework. More accurate calculations, for example, full wave calculations accounting for the inhomogeneity or calculations incorporating kinetic theory effects are beyond the scope of this work.

Writing the solution to equation (1) in separable form, $E(r, \phi) = R(r)\Phi(\phi)$, we obtain the expression

$$\frac{r}{R}\frac{d}{dr}\left(r\frac{dR}{dr}\right)+k_\perp^2(r)r^2=-\frac{1}{\Phi}\frac{d^2\Phi}{d\phi^2}=m^2\,.$$

The periodic solution in the interval $0 \le \phi \le 2\pi$ with integer $m = 0, 1, 2, \ldots$ is

$$\Phi(\phi)\sim\exp(\pm im\phi)\,.$$

Hereafter m is referred to as the azimuthal quantum number. The radial part of the equation becomes then

$$\frac{1}{r}\frac{d}{dr}\left(r\frac{dR}{dr}\right)+\left[k_\perp^2(r)-\frac{m^2}{r^2}\right]R=0\,. \tag{3}$$

To proceed requires matching the eikonals across the wave-turning point. For a cylindrical density column, if only one turning point r_0 is found the matching condition is applied across a pair of symmetric turning points r_0 on opposite sides of the column centered around the axis,

$$\int_{-r_0}^{r_0}dr\left[k_\perp^2(r)-\frac{m^2}{r^2}\right]^{1/2}=2\int_0^{r_0}dr\left[k_\perp^2(r)-\frac{m^2}{r^2}\right]^{1/2}=\left(n+\frac{1}{2}\right)\pi\,. \tag{4}$$

On the other hand, in the presence of two turning points, say r_1 and r_2, the matching condition is applied across both of them:

$$\int_{r_1}^{r_2}\left[k_\perp^2(r)-\frac{m^2}{r^2}\right]^{1/2}dr=\left(n+\frac{1}{2}\right)\pi\,. \tag{5}$$

Equations (4) and (5), whichever applies, determine the radial quantum number n and are hereafter referred to as the quantization condition.

The eigenfrequencies can be determined only after assuming a geometry for the density variation that traps the waves. For simplicity, we model this density variation as a "waterbag" model; assuming a square density profile,

$$n(r) = \begin{cases} n_0 & \text{for } r > L\ , \\ n_0(1+\delta) & \text{for } r < L\ . \end{cases} \tag{6}$$

It is shown in Appendix A that, similar to whistler waves, upper hybrid Z-mode waves can be trapped only in density enhancements. Thus local irregularities in density must be density increases to trap the upper hybrid mode and cause zebra emission. The integrand of the quantization condition in equation (4) or (5) then transforms into

$$\begin{aligned} k_\perp^2 - \frac{m^2}{r^2} &= \frac{2}{\rho_e^2}\frac{\Omega_{ce}^2}{\omega^2\omega_{p0}^2}(\omega_{\min}^2 - \omega^2) - \frac{m^2}{r^2} \quad (r > L)\ , \\ &= \frac{2}{\rho_e^2}\frac{\Omega_{ce}^2}{\omega^2\omega_{p0}^2}\frac{\omega_{\max}^2 - \omega^2}{1+\delta} - \frac{m^2}{r^2} \quad (r < L)\ , \end{aligned} \tag{7}$$

where $\omega_{\min}^2 = \omega_{p0}^2 + \Omega_{ce}^2$ and $\omega_{\max}^2 = (1+\delta)\omega_{p0}^2 + \Omega_{ce}^2$ are the upper hybrid frequencies outside and inside the waterbag, respectively. From the above result, it is easy to see that the frequency range defined by the inequality $\omega^2 > \omega_{\max}^2$ corresponds to a forbidden band.

Henceforth, we consider only modes with finite m, and we define dimensionless versions of the critical variables: $\rho = \rho_e/L$, $\alpha = \omega_{p0}/\Omega_{ce}$, $x = \omega/\Omega_{ce}$, and $y = r/L$. This allows us to rewrite equation (7) as

$$\begin{aligned} Q^2(y) &\equiv k_\perp^2 L^2 - \frac{m^2 L^2}{r^2} \\ &= \frac{2}{\rho^2}\frac{1 + (1+\delta)\alpha^2 - x^2}{(1+\delta)\alpha^2 x^2} - \frac{m^2}{y^2} \quad (y < 1)\ , \\ &= \frac{2}{\rho^2}\frac{1 + \alpha^2 - x^2}{\alpha^2 x^2} - \frac{m^2}{y^2} \quad (y > 1)\ . \end{aligned} \tag{8}$$

The turning points are obtained by solving the equation $Q(y_*) = 0$, with the ranges of x^2 and m restricted as described in Appendix A. Solving for y_*, we obtain

$$y_* = \frac{m\rho}{\sqrt{2}}\frac{(1+\delta)^{1/2}\alpha x}{[1 + (1+\delta)\alpha^2 - x^2]^{1/2}}\ . \tag{9}$$

In terms of y_* and considerations of Appendix A, the quantization condition in equation (5) becomes

$$\int_{y_*}^{1} Q(y)\, dy = \left(n + \frac{1}{2}\right)\pi\ , \tag{10}$$

which can be explicitly rewritten as

$$\begin{aligned} I &\equiv \int_{y_*}^{1} dy \left[\frac{2}{\rho^2}\frac{1 + (1+\delta)\alpha^2 - x^2}{(1+\delta)\alpha^2 x^2} - \frac{m^2}{y^2}\right]^{1/2} \\ &= \left(n + \frac{1}{2}\right)\pi\ . \end{aligned} \tag{11}$$

This integral can be solved analytically (see Appendix B). The solution for fixed n, which is the desired dispersion equation for the discrete eigenmodes, is

$$\zeta_m - \arctan\zeta_m = \frac{(2n+1)\pi}{2m}\ , \tag{12}$$

where

$$\zeta_m = \left[\frac{2}{m^2\rho^2}\frac{1 + (1+\delta)\alpha^2 - x^2}{(1+\delta)\alpha^2 x^2} - 1\right]^{1/2}\ , \tag{13}$$

$n = 0, 1, 2, \ldots$ are arbitrary integers, and m is an integer greater than 1, which is subject to the constraints derived in Appendix A. The main constraint given in equation (A2) restricts the number of harmonics to $m < \sqrt{\delta}/\rho$, showing that the maximum number of harmonics depends essentially on the small parameter ρ. Consequently, for a column size L much larger than the electron gyroradius ρ_e the number of harmonics can be quite large. Expecting maximum density increases of the order of $\delta < 1$, the number of harmonics becomes $m < \rho^{-1}$, which implies that for a not unreasonable value of $\rho \sim 0.01$, the harmonic number m may approach $m \sim 100$. Further discussion on this point can be found in the following section and in Appendix A.

4. APPLICATION TO ZEBRA EMISSIONS

It is straightforward to solve equation (11) numerically for the eigenfrequencies $x = f/f_{ce}$ for selected parameters. We consider two choices for $\alpha = f_{pe}/f_{ce}$, $\alpha = 1.7$, corresponding to the double-resonance condition $f_{uh} = 2f_{ce}$, and $\alpha = 2.8$, corresponding to the triple-resonance condition $f_{uh} = 3f_{ce}$. These are the two conditions for which the mechanism appears to operate in the terrestrial auroral ionosphere, so we start by assuming these conditions for the solar corona as well. Figures 3 and 4 show numerical solutions of equation (11) for these two choices of f_{pe}/f_{ce}, for $\delta = 0.2$, corresponding to 20% density enhancements, and for $\rho = \rho_e/L$, the ratio of the electron gyroradius to the

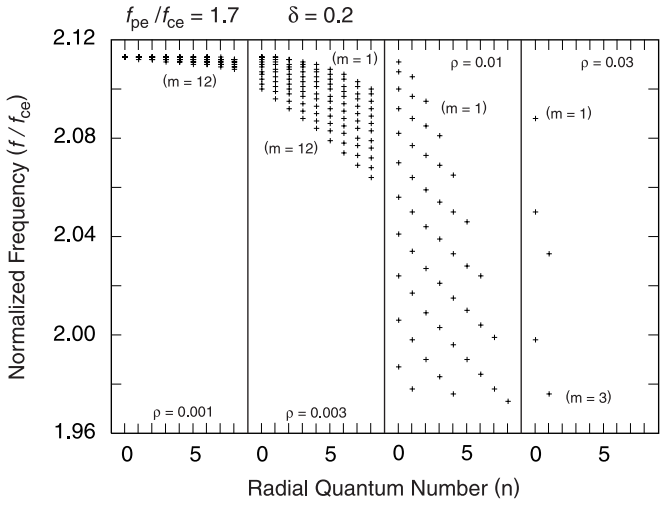

FIG. 3.—Eigenfrequencies of upper hybrid cavity modes in a 20% field-aligned cylindrical density enhancement for $f_{pe}/f_{ce} = 1.7$ ($f_{uh} = 2f_{ce}$). Frequencies for each of 10 radial quantum numbers (n) and up to 12 azimuthal quantum numbers (m) are calculated for four cavity dimensions ($\rho = \rho_e/L = 0.001, 0.003, 0.01$, and 0.03). The eigenfrequencies are normalized to the electron gyrofrequency. Frequency spacings on the order of 1% occur for $\rho = 0.01$–0.03.

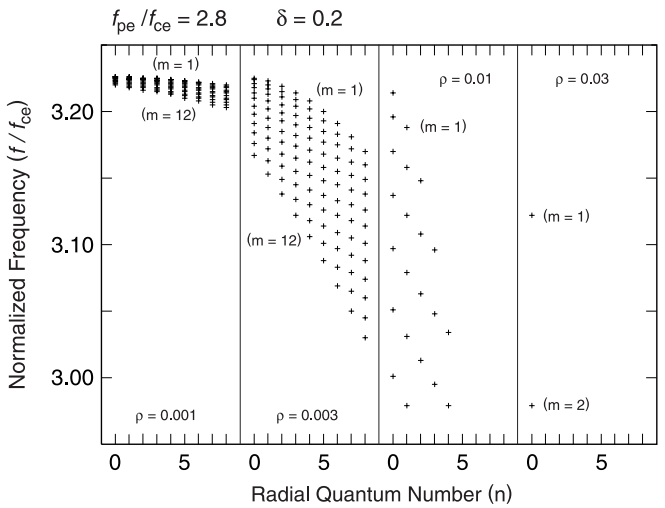

FIG. 4.—Eigenfrequencies of upper hybrid cavity modes in a 20% field-aligned cylindrical density enhancement for $f_{pe}/f_{ce} = 2.8$ ($f_{uh} = 3f_{ce}$). Frequencies for each of 10 radial quantum numbers (n) and up to 12 azimuthal quantum numbers (m) are calculated for four cavity dimensions ($\rho = \rho_e/L = 0.001$, 0.003, 0.01, and 0.03). The eigenfrequencies are normalized to the electron gyrofrequency. Frequency spacings on the order of 1% occur for $\rho = 0.01$–0.03.

radius of the density enhancement, ranging from 0.001 ($L = 1000\rho_e$) to 0.03 ($L \approx 30\rho_e$). For each case, the normalized eigenfrequency ($x = f/f_{ce}$) is shown on the y-axis for the first 10 radial quantum numbers ($n = 0, \ldots, 9$). For each radial quantum number, only solutions for up to 12 azimuthal quantum numbers (m) are shown, although fewer m-numbers are shown for cases for which the range of m is restricted by the constraints given in equations (A1) and (A2).

From the numerical results it is evident that if all combinations (n, m) are included, values of ρ in the range 0.01–0.03 lead to spacings in the normalized eigenfrequencies on the order of a few percent, corresponding to the observed zebra band spacings of a few megahertz at metric wavelengths and a few tens of megahertz at decimetric wavelengths (Figs. 1 and 2). This result implies density enhancements with scale sizes 30–100 times the electron gyroradius. Turning to the decimetric example (Fig. 1), matching the emission frequency of ~1.4 GHz to the double-resonance condition implies $f_{ce} = 700$ MHz or $B = 270$ G. For a temperature of 1 keV, the electron gyroradius is about 25 cm. Therefore 1–10 m scale field-aligned irregularities of order 20% would be required to explain the observed type IV zebra spacings as resulting from eigenmodes of trapped upper hybrid waves generated by the cyclotron maser mechanism at the double-resonance condition. Admittedly, such strong density contrasts seem unreasonably high, and below we will strongly relax the requirement of density fluctuation amplitudes so high. Incidentally, calculations show that less severe density enhancements, of order 1%–5%, are also effective in forming discrete eigenmodes in meter-scale enhancements, but one expects that fewer eigenmodes could satisfy the restrictions in Appendix A, equation (A2). This restriction, however, is not important as the number of harmonics is determined by ρ rather than the density contrast, δ. The latter can be made much smaller for shallow density structures and still will cause a large number of harmonics for small ρ. As described in Appendix A, the temperature plays an important role in determining how many discrete eigenmodes occur, because the ratio of the width of the density enhancement to the gyroradius determines the number of allowed azimuthal modes for each radial quantum number n. As discussed at the end of the previous section, for small ρ and wide density enhancements, on the order of tens of meters rather than meters, large numbers of zebra stripes may be expected.

The above range of values, $\rho \sim 0.01$–0.03, indeed implies large m even for moderate density increases. For instance, with $\delta \sim 0.2$, the maximum harmonic number is $m_{\max} = 44$ for $\rho \sim 0.01$, and $m_{\max} = 15$ for $\rho \sim 0.03$, and larger density increases lead to even larger $m_{\max}$. In the 270 G magnetic field the gyroradius of a 1 keV electron is 25 cm, which for $\rho \sim 0.01$ yields $L \sim 50$ m for the radial extension of the column of enhanced density, still extremely narrow compared with the radial size of a type IV magnetic loop. Hence, such small ρ values are not at all unreasonable.

Examples of simultaneous sets of zebra emissions on widely spaced frequencies, such as the zebra features near 1.0–1.4 and 2–3 GHz shown by Ledenev et al. (2001), can be explained as arising either from the double-resonance condition met in two rather widely spaced source regions characterized by a factor of ~2 in differing magnetic field and plasma density environments or from different resonance conditions being met at locations where the magnetic field is slowly varying but the electron density varies by factor of ~2, leading, for example, to $f_{uh} = 2f_{ce}$ for one branch of zebras and $f_{uh} = 3f_{ce}$ or $f_{uh} = 4f_{ce}$ for the other branch. This latter situation is analogous to the sources in the terrestrial auroral ionosphere for which auroral roar emissions occur simultaneously at frequencies near 3 MHz ($f_{uh} = 2f_{ce}$) and near 4.5 MHz ($f_{uh} = 3f_{ce}$).

The theory given here, based on the simplified "waterbag" model of the density enhancement, predicts that the zebra emissions originate from remarkably compact sources, as small as 1 m scale or 10 m scale. Consideration of more complex shapes of the density enhancement may yield some shapes that imply a somewhat larger source. It is, however, unlikely that a more complicated (more realistic) density profile of the striation will affect the result by a large amount. The theory is rather robust with respect to a variation of the profile. The strikingly small source size implied by the theory raises three important questions: (1) whether there is sufficient energy for such a source to feed into the emission, (2) whether such a compact source is stable for a sufficiently long time to explain zebra emissions that last ~10 s or longer, and (3) whether such a compact source is consistent with radio images of type IV bursts, in other words, whether it could ever be resolved by remote sensing and imaging instrumentation.

4.1. *Radiation Intensity*

Assuming zebra bursts subtend solid angles ~1 sr, have bandwidth ~10^6 Hz, and are observed with intensity 500 sfu (500×10^{-22} W m^{-2} Hz) at 1 AU as in Figure 1, the power at the source must be of order 10^9 W in each single zebra harmonic line. Hence, the total zebra emission, depending on the number of harmonics, may range from a few times 10^9 to ~10^{11} W (assume 10^{10} W in calculations below). This power comes ultimately from the energy of the electrons trapped on the field lines intercepting the source. According to our model, the radius of the density enhancement that

traps the upper hybrid waves is 1–10 m, implying a source dimension perpendicular to the magnetic field of 3–300 m^2 (assume 30 m^2 in calculations below). If the temperature of the trapped electrons is of the order of 1 keV (1.6×10^{-16} J), then the number flux required to produce 10^{10} W is $\sim 3 \times 10^{24}$ m^{-2} s^{-1}. For 1 keV electrons the thermal velocity of $\sim 1 \times 10^7$ m s^{-1} implies an electron density of 2×10^{17} m^{-3}, or 2×10^{11} cm^{-3}, required for the electron energy per time entering a single narrow source region to match the emitted wave power. The estimated conditions at the source, $f_{pe}/f_{ce} = 1.7$ in a 270 G field, imply a total electron density of 2×10^{10} cm^{-3}, a factor of 10 smaller than that required to produce the observed wave power, even assuming all electron energy goes into radiating waves; therefore this mechanism cannot account for the emitted power of the zebra bands on the basis of a single density enhancement as the single source. Rather one needs many sources. We will argue below that many sources favor the reality of this mechanism.

That a single 10 m scale source cannot be responsible for the zebra emission is not surprising and also not required. The smallness of the source compared with the dimensions of a coronal magnetic loop suggests that a very large number of those microscopically small density irregularities, fitting in a tiny region of the loop, generate the zebra emissions. Figure 5 shows a schematic of the zebra emission region proposed. Three characteristics of the source volume are critical: first, the altitude range spanned by the source volume must be small so that the average electron density and magnetic field are approximately the same for all the sources; second, the density enhancements should all be approximately of the same size so that the trapped mode frequency structure for each is approximately the same; and third, the density contrast in the enhancements must be of the same approximate magnitude to contribute to about the same number of harmonics. The second criterion could easily be met, for example, if the density irregularities are associated with low-frequency electrostatic modes such as ion-acoustic waves excited within a relatively narrow range of wavenumber space. If the low-frequency waves composing the density enhancements had too broad a wavenumber spectrum, the emissions from the trapped waves in the enhancements would start overlapping and would cause continuum emission rather than zebra emissions. The third criterion implies that the spectrum of density irregularities should peak around a most probable amplitude.

To consider the required number and packing density of such sources, let us assume a mode conversion efficiency of 1%, comparable to the mode conversion efficiency estimated for emission of terrestrial continuum radiation at the Earth's plasmapause by a similar mode conversion process to that required here (e.g., Etcheto et al. 1982). We assume

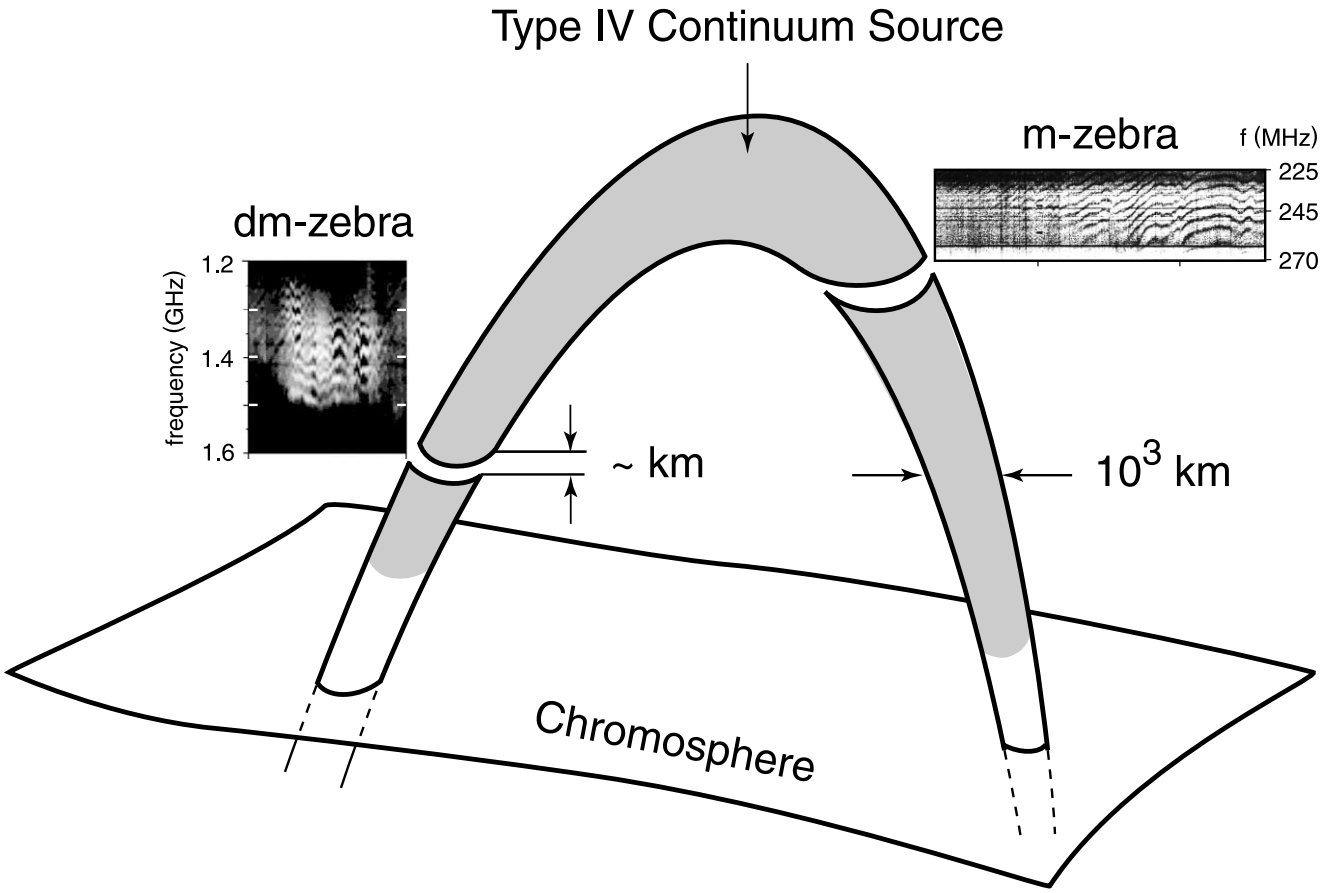

FIG. 5.—Schematic model of a zebra emission region in type IV solar radio bursts. The type IV continuum is generated by the trapped particle distribution. The figure shows two source regions of zebra burst emission, one in the decimetric domain at low altitudes above the chromosphere, the other in the metric domain at higher altitudes. It is assumed that these regions are at constant altitudes, filled with (e.g., ion acoustic) density irregularities. Variations and motions of these source regions cause the slow simultaneous frequency variations of the zebra bands.

further that the hot electrons give up 0.01% of their energy to electrostatic upper hybrid waves in passing through the source region. This implies a factor of 10^{-6} between electron power and wave power. If the hot trapped component of the total electrons amounts to only 10%, then the total electron density in the source region (2×10^{10} cm^{-3}) and the source size of $\sim$30 m^2 imply that approximately 10^8 such sources are required to produce the observed power of the zebra emissions. Even with a tiny filling factor this quantity of emissions can fit within a volume small compared with a coronal loop; for example, a filling factor of 0.01 requires that the cross-sectional area containing the 10^8 sources be 3×10^{11} m^2 or only 500×500 km, roughly 10% or less of a loop cross section. It is essential that the sources occupy a small altitude range, so that the electron density and magnetic field strength be approximately constant over the entire volume permeated by these sources. Another way of expressing this calculation is the following: suppose the sources inhabit an altitude range of only 10 km but a cross-sectional area of about 1000 km radius. The corresponding source volume is about 10^{16} m^3, giving room for 3×10^9 individual sources of cross section 30 m^2 with a packing factor of 0.01, or 10^8 if a packing factor of 0.001 is assumed. To produce total emission of 10^9–10^{11} W, each source would need to radiate 10–1000 W, the high end of which would require an electron number flux of $\sim 3 \times 10^{24}$ m^{-2} s^{-1}, assuming 1 ke V source electrons, 0.01% efficiency for electrons in upper hybrid waves, and 1% efficiency for mode conversion; this yields the number flux estimated above for the source conditions in the coronal loop.

The assumption of many microscopic sources in zebra emission raises the question of the coherence of the radiation. Of course, the sources need not be phase coherent as in a laser but only need be coherent in the sense that they must produce the same frequencies. As long as the sources are confined to a narrow layer within the type IV magnetic loop, which is of order 1–10 km high and of radius 500–1000 km as described above, in such a layer the altitude variation of the loop magnetic field and the electron density can be neglected. The whole layer acts like a single emitter since the differences in the emissivity among the single radiators cannot be resolved. Moreover, the individual density increases affect mainly the individual numbers of harmonics radiated while for the same plasma and cyclotron frequencies they all contribute to the same emission lines though at possibly different times. The other critical criterion to produce zebra rather than continuum type IV emission is that the sources all have similar dimensions perpendicular to the magnetic field; this condition would hold, for example, for density irregularities associated with ion sound waves of a restricted wavenumber spectrum.

Differences in the velocities of the individual emitters along the magnetic field contribute to broadening of the zebra emission lines. Measuring the width of each line provides a measure of the average velocities of the single emitters along the loop magnetic field lines. To obtain an impression we assume that the density irregularities are essentially caused by ion-acoustic fluctuations in the loop plasma, which may be excited by field-aligned currents, heat fluxes, ion beams, or other mechanisms. The common property of such irregularities is that they propagate mostly along the magnetic field at the ion acoustic speed, $c_{ia} = (\gamma k_B T_e / m_i)^{1/2}$, where $\gamma k_B T_e$ is the electron thermal energy, γ the adiabatic index, and m_i the ion mass. For $k_B T_e \sim 1$ keV, the ion acoustic speed is $c_{ia} \sim 310 (m_p/m_i)^{1/2}$ km s^{-1}, where m_p is the proton mass. The localized density enhancements in this mode propagate at speeds well below c_{ia}. Assuming that the $\Delta f \sim 2$ MHz bandwidth associated with metric zebra bands (Fig. 2) is produced by thermal Doppler shift broadening, the typical extension of an individual radiation source along the magnetic field must be $\lambda \sim 2\pi c_{ia}/\Delta f$, about several meters. In ion sound wave turbulence the perpendicular scales are of the same order or up to an order of magnitude longer, which is in agreement with our previous estimates of the scale of the microscopic density irregularities. Also, the bandwidth of the single zebra bands falls well into the domain of frequencies below the local ion plasma frequency $\Delta f < f_{ci} = (m_e/m_i)^{1/2} f_{pe}$, which is another condition for ion-acoustic waves to be involved.

Apparently, an important restriction is imposed by the assumed large amplitude in the density variation, which is of the order of some $\delta \sim 10\%$, implying very strong density fluctuations and a large density contrast, indeed. It seems entirely unlikely that any ion-acoustic or other electrostatic plasma mode would produce solitary structures of amplitudes that large. Ion-acoustic soliton amplitudes are expected to range around 1% or even smaller. It is desirable to reduce the high density contrast to more realistic values. This can be easily done with little consequence when noting that for large numbers $\rho \gg \delta$ of electron gyroradii that fit into one striation length L the number of harmonics is determined mainly by ρ and is proportional to δ. Small δ thus imply a linear reduction of the number of zebra bands. However, in the case of ion-acoustic solitary density striations there is an inverse proportionality between δ and L (e.g., Horton & Ichikawa 1996). Large density contrasts imply narrow striations, small contrasts imply shallow striations. The smaller the density contrast, the wider the striation and, consequently, the greater the number of electron gyroradii that fit into it. This property compensates for the decrease in the number of harmonics. One therefore finds that at the small reasonable density contrasts, the number of harmonics will not change remarkably but remains approximately constant. On the other hand, widening the striations reduces the absolute number of density structures that can be fitted into the macroscopic radiation source region in our model. Referring to the above estimates, we conclude that the model proposed here is rather insensitive to the reduction of the total number of striations. Reducing the large filling factor estimated above even by an order of magnitude does not imply any serious violation of our general conclusions that many striations are needed to be present in the zebra source.

The zebra emission mechanism proposed in this paper is a coherent one. It raises the question of whether or not coherence is demanded by observation of high radiation power corresponding to extreme brightness temperatures or whether it is merely concluded from observation of the narrow spectral bandwidths and "coherent" variations of the observed zebra frequency bands. The present model solely refers to the latter, while the radiation intensities and brightness do not explicitly enter other than in the above discussion of the energy source. Hence, our "coherence" is strongly model-dependent. The observations of, say, fluxes of $\sim$500 sfu at $\sim$1 GHz in a zebra line correspond to a brightness temperature of not more than $T_b(1\ \mathrm{GHz}) \approx 5 \times 10^4$ K, suggesting high thermal but indeed not extraordinarily high coherent brightness temperatures in zebra

bands, thus not making an inherently coherent radiation mechanism inevitable. The radiation intensities are moderately enhanced only over the type IV background that is known to be produced by an incoherent mechanism. However, the mechanism proposed here does not necessarily imply that continuum and zebra emissions are generated by the same process. It is indeed required only that in the region of interest upper hybrid waves that can be trapped in density irregularities are excited. This is grossly independent of any mechanism that generates the type IV continuum.

4.2. *Nature of the Continuum*

In this paper we assumed that the radiation is produced by some mechanism that is independent of the formation mechanism of zebra emissions. As such a mechanism we proposed that Z-mode (upper hybrid) waves are excited by the electron cyclotron maser mechanism in dense plasma as originally suggested by Winglee & Dulk (1986). Their theory is well suited for a homogeneous plasma, however. It is not known how it works under the conditions relevant to our case, in which the dense background plasma is assumed to be locally in a highly turbulent state with a very large number of small-scale density striations superposed on the background plasma and these striations are slowly moving ion-acoustic solitary structures of weak amplitudes $\delta \leq 1\%$. In plasmas of this kind it has been shown by Fleishman & Kahler (1992), Fleishman & Tokarev (1995), and Fleishman (2001), referring to earlier suggestions (e.g., Ginzburg & Tsytovich 1984), that energetic particles moving across a turbulent plasma with a spectrum of density inhomogeneities emit so-called transition radiation at frequencies above the average local plasma frequency $\omega > \omega_{pe}$. For nonrelativistic particles this radiation is emitted in both modes, the L-O and R-X modes, such that the radiation will essentially be nonpolarized and only weakly polarized in the L-O-mode near the plasma frequency. Indeed, type IV radiation is grossly nonpolarized and would fit into this class of radiation. This suggests that the observed background in events when zebra emission is present and is generated by our turbulent mechanism could result from transition radiation.

For an estimate of the relevance of this assumption we refer to the presentation of the mechanism of transition radiation as given by Fleishman (2001). The case applicable to the conditions in a zebra burst is described by equation (25) of Fleishman (2001), with relativistic factor $\gamma \sim 1$ for electrons of energy 1–10 keV. Introducing the electron skin length $\lambda_e = c/\omega_{pe}$ we write the expression for the transition radiation radio flux at Earth (in sfu) in the form

$$F_{TR}(\omega) = 6\pi \times 10^4 C \frac{\omega_{pe}}{2\pi\ \mathrm{GHz}} \frac{N_>}{10^{33}} \frac{m_e c^2}{k_B T_e} \times \left(\frac{\omega_{pe}}{\omega}\right)^{\alpha_f} \delta^2 \gamma^{\nu+2} \left(\frac{2\pi\lambda_e \rho}{r_{ce}}\right)^{\nu-1} . \quad (14)$$

The flux decreases with increasing emitted frequency ω and electron temperature being maximum close to ω_{pe}. It increases with density contrast δ and ρ, the number of gyroradii fitting into one density striation. It also increases with the total number of energetic electrons $N_>$ above thermal energy. In addition, for relativistic electrons it increases as a power of γ.

The constant C in the above expression is a combination of the power-law indices entering the theory of transition radiation. These indices are the index ν_δ of the distribution of the density contrast, index ξ of the suprathermal electron distribution, and the above index α_f. Fleishman (2001) has shown that $\alpha_f \approx 3$, and for developed nonrelativistic turbulence $\nu_\delta \approx \frac{5}{3}$ is about Kolmogorov. Since in the case of type IV zebra emissions there is no indication for the presence of very energetic electrons, the electron spectrum is soft, with a large power-law index $\xi \sim 6$–7. In this case it can be shown that $C = \mathcal{O}(1)$. With the parameters used in this paper, $5 < \lambda_e/r_{ce} < 50$.

Adopting the value for $N_> \sim 10^{32}$ as estimated by Fleishman (2001), we thus obtain for the continuum flux in transition radiation in typical zebra events

$$F_{TR}(\omega) \sim 6 \frac{N_>}{10^{32}} \left(\frac{\delta}{1\%}\right)^2 \left(\frac{\rho}{10^{-3}}\right)^{2/3} \mathrm{sfu} . \quad (15)$$

This flux is in the range of weak continuum radiation conditions. Fluxes up to 2 orders of magnitude higher can be expected for larger density increases and larger numbers of irregularities, explaining strong type IV backgrounds generated by transition radiation.

We may thus conclude that transition radiation in the ion-acoustic solitary structure (density striation) turbulent state investigated in the present paper is obviously important and can essentially contribute to the enhanced background observed in zebra emission. It should be noted in this context that recently Lee et al. (2003) found evidence for transition radiation in microwave observations during a solar flare.

There is another very interesting aspect concerning the transition radiation contribution mentioned in this subsection. The transition radiation is emitted just above the electron plasma frequency. Since this is close though less than the upper hybrid frequency the part emitted in the R-mode actually propagates in the Z-mode, and close to the upper hybrid frequency it is mainly electrostatic. Hence, there arises the possibility that transition radiation may as well generate sufficient intensity in the upper hybrid branch to be trapped in the density striations and generate zebra emissions. If this is the case transition radiation and zebra emission are even more closely coupled than by the presence of ion-acoustic solitary turbulence as the latter makes possible both transition radiation and zebra emission resulting from transition radiation.

4.3. *Stability of Sources*

Small-scale structures such as those proposed here are conventionally believed to suffer rapid destruction by the energetic electron component trapped in the loop. Indeed, the mean free path of an electron in a solar coronal loop under conditions of type IV radio bursts is many orders of magnitude larger than the size of the density enhancement both parallel and perpendicular to the magnetic field, which seems to suggest that the density enhancement should be wiped out by the diffusive motion of the electrons. However, this is not necessarily the case in a collisionless plasma as assumed here.

There is little problem with the perpendicular stability of the individual structures because the electron gyroradius is much less than the perpendicular dimension of the density enhancement. Perpendicular diffusion of electrons is rather slow (see, for example, Treumann, LaBelle, & Bauer 1995),

usually much less than the maximum Bohm diffusion limit, $D_B = k_B T_{e\perp}/16\pi m_e B$, where k_B is Boltzmann's constant, $T_{e\perp}$ the perpendicular electron temperature, and B the magnetic field. For electron temperatures a few times 10 keV and magnetic fields on the order of a few hundred gauss, Bohm diffusion is about $D_B \approx 10^4$ m^2 s^{-1}. For a structure of perpendicular length L to survive a time τ one has $L = (D_B\tau)^{1/2}$, implying that 300 m wide density enhancements are required to survive $\tau = 10$ s while suffering Bohm diffusion. However, theory and in situ measurements in the Earth's magnetosphere have shown that Bohm diffusion strongly overestimates the collisionless diffusion limit by roughly 2 orders of magnitude. If similar scaling applies to the collisionless plasma in the solar coronal loops, meter-scale or somewhat larger density enhancements would survive for a time on the order of 10 s. Moreover, our conclusion that many such microscopic radiators are present liberates us from the restriction of long survival as a decaying radiator will readily be replaced by another one that is just generated by the process that generates the irregularities.

Parallel to the magnetic field, the question is more complicated and concerns the stability of relatively long-lived localized irregularities in collisionless plasmas, where in the absence of collisions the particles simply undergo free streaming. Under these conditions many mechanisms lead to formation of spatially localized quasi-stationary density irregularities, so called solitary structures, as well as Bernstein-Green-Kruskal or BGK modes (e.g., Davidson 1972), which are stable over many plasma and gyroperiods. Examples of such structures are Korteweg–de Vries solitons, ion-acoustic solitons, drift wave solitons (e.g., Horton & Ichikawa 1996), and also ion holes (e.g., Gray et al. 1991) and electron holes (e.g., Muschietti et al. 1999). Since here we are interested only in density enhancements, the most promising of these quasi-equilibria are either ion-acoustic or drift wave solitary structures, either of which could explain the scale size and lifetime of type IV sources. Their stability against depletion by the trapped particle component in the loops is maintained by a subtle temporary equilibrium either between the dispersive properties of the waves and the trapped particle dynamics or between the trapped wave pressure and plasma pressure. These structures endure only in hot collisionless plasma where collisions are inhibited to such an extent that either trapping of some low-energy particles in the wave potential becomes possible or the dispersive properties of the waves involved are not inhibited by collisional damping. The detailed application of these theories to the hot plasma in the coronal loop is beyond the scope of this paper, other than noting that the theories do apply there, and it is reasonable to assume that sufficiently long-lived density enhancements occur.

At this point a caveat related to the amplitude of the density enhancement should be pointed out. We have so far used local density increases δ of the order of $\sim$20%, which is a high value. In a mechanism such as that of Treumann & Bernold (1981) on the basis of nonlinear whistler theory it would be very hard to achieve local density increases of this size. This difficulty is related to the electromagnetic nature of the whistler, which requires substantial bending of the magnetic field in accord with a density increase that thus can be excluded in a $\beta \ll 1$ plasma like that of the loop. In the case considered here, $\beta \sim 3 \times 10^{-3}$. Substantial density variations are generated solely by electrostatic waves like the ion-acoustic wave mode used above, in which the density increase $\delta \approx e\Delta\Phi/\gamma k_B T_e$ is given by the potential energy $e\Delta\Phi$ in the electrostatic wave normalized to thermal energy. With $\gamma k_B T_e \sim 1$ keV this implies an average ion-acoustic electric field strength of $(\langle E_{ia}\rangle 1200/L)$ V m^{-1}, where L is in meters. This is still high. Thus, one should rather use smaller density variations of the order of 1% or less, which implies that the number of harmonics contributed by the sources will be reduced to only a few. Hence, in spite of our initial discussion, the number of zebras is still restricted to a relatively small number; for $\delta \sim 2\%$ it is $m < 10$, unless the structures are wider or high ion-acoustic wave electric fields are present in the source region, which cannot be entirely excluded, however. Such large density irregularities are familiar in the Earth's upper ionosphere, where at magnetic field strengths of only 10^{-3} G and $\beta \sim 0.1$ wave amplitudes between 0.1 and 1 V m^{-1} are measured. In view of these numbers the above wave amplitudes do not look too unreasonable. Moreover, we can without running into difficulties relax the restriction on the extension of the density structures. For $L \sim 100$ m the average electric field amplitude would then become on the order of $\langle E_{ia}\rangle \sim 10$ V m^{-1}. By observing large harmonic numbers one concludes either that the structures are wider or the average electric field amplitudes in the ion-acoustic modes are larger.

4.4. *Spatial Resolution*

Ground-based imaging observations at metric wavelengths tend to associate type IV emissions with relatively large source sizes, comparable to the size of the entire coronal loop. For example, Chernov et al. (1998) present imaging results on a structured type IV burst by using the Nançay radioheliograph (their Fig. 3). The suggested source size is large and centered between two active regions simultaneously imaged with the *Yohkoh* satellite, suggesting a type IV source that is extended high in the coronal part of the active loop. In this observation no zebras are resolved spatially. In a follow-up observation Chernov et al. (1999) present an image of another type IV burst, noting "two remarkable peculiarities...: The source of the zebra-patterns was located above the filament far (>8′) from the source of the strong continuum, [and] strong changes in position of zebra-lines and pulsations were observed. The most common property of the zebra-patterns in all the considered events should be the displacement between the sources in emission and ones in absorption. The average distance should be of about 50,000 km. Great dimensions of the source were observed for the isolated zebra-lines, comparable to the FWHM of the beam (about 2′ at 236.6 MHz) ... however such dimensions are rather similar to the scattering size of the electromagnetic waves in the corona .... However sources of zebra patterns were not deconvolved completely by the Nançay radioheliograph (the source size was similar to the FWHM of the beam at 236.6 MHz)." These remarks indicate the difficulty and uncertainty in imaging the zebra patterns and determining their location and size from such an image in the solar corona. To our knowledge, zebra patterns have not been convincingly imaged yet. Obviously it represents an enormous experimental challenge to identify source sizes as small as those we put forth here even for multiple sources filling a substantial cross section of a loop.

However, if the observation of extended source sizes cited above pertains to the zebra emission rather than the continuum, the physical source size of the zebra features is not significantly constrained by it. Observation of an extended source implies most likely that the radio emission from the source on its way to the Earth is multiply scattered and that the apparent size of the source is thereby considerably enlarged. This interpretation is supported by the observation of Chernov et al. (1999) that the apparent source size compares with the typical scattering dimensions of radio waves in the corona.

5. CONCLUSIONS

Solar type IV emissions have a complicated nature, consisting sometimes of a continuum, but at other times exhibiting fine structures variously called fibers, spaghetti, zebras, etc. In this way, they are similar to terrestrial auroral roar emissions, which also sometimes consist of continuum, but at other times they show fine structures, including "multiplet" structures, which resemble the type IV zebra emissions. This similarity inspires us to propose that type IV emissions may be generated by a similar mechanism that generates the terrestrial auroral roar. The basic mechanism is that proposed previously by Winglee & Dulk (1986): in the presence of trapped electron distributions, the cyclotron maser mechanism leads to growth of Z-mode waves that close to the upper hybrid frequency become electrostatic. Here they can produce radio emission when meeting the double-resonance condition $f_{uh} = Nf_{ce}$, where N is an integer ≥ 2. In our treatment the zebra structures are not caused by different values of N. Instead, we put forth that type IV zebra emission arises from the double-resonance condition in a hot electron plasma occurring over an extended region. When density irregularities are weak or absent, or when these are of inappropriate scale for causing a discrete spectrum of density striation trapped upper hybrid eigenmodes, continuum radiation may be generated. However, when density enhancements of the appropriate scale occur, these trap the cyclotron maser–produced Z-mode waves propagating in the upper hybrid frequency branch and impose a discrete trapped-mode eigenstructure on them. Escaping mode-converted waves retain the discrete frequency structure of these trapped modes. In this case, the local type IV emission appears as discrete fine-frequency structures, such as zebra bands. Separate instability of the trapped eigenmodes is not required. The presence of the density striations then simply removes the degeneracy of the upper hybrid wave. To produce the radiation it is further assumed that the mode conversion at double resonance does not distinguish between the single eigenharmonics of the trapped waves as their separation in frequency space is very small in comparison with the upper hybrid frequency and probably also small compared with the bandwidth of the double resonance.

Quantitative calculation of the spacing of the eigenfrequencies of the trapped waves near the double-resonance condition shows that for density enhancements with scale sizes 30–100 times the electron gyroradius the frequency spacing between eigenmodes is of order of 1% as in the observations. In a 1 keV plasma with a 270 G magnetic field, this corresponds to a 1–10 m scale. We have noted that the number of harmonic zebra bands for shallow density contrasts depends essentially on the number of electron gyroradii fitting into the density striation. If the density enhancements are ion-acoustic soliton-like, arising from dispersive ion-acoustic waves, their wavenumber range inferred from interpreting the width of the zebra emissions as Doppler broadening matches the 1–10 m scale size required by the theory. For such ion-acoustic soliton striations the number of harmonics increases with increasing shallowness, implying that the number of harmonics in one striation is about constant, independent of the density contrast $\delta \ll 1$.

However, a 1 m scale or 10 m scale source in a 1 keV coronal plasma cannot reproduce the observed radiation intensities. Instead a large number ($\sim 10^7$–10^8) of microscopic emitters distributed over a substantial portion of a loop cross section and confined to a narrow altitude range along the loop easily accounts for the observed radiation power. To produce the banded zebra signatures, it is critical that these sources inhabit only a narrow altitude range, hence corresponding to approximately the same magnetic field and average plasma density, and that the causative electron density enhancements have similar average dimension perpendicular to the magnetic field, as would be the case, for example, if they originated from the above-mentioned ion-acoustic waves of restricted bandwidth. When these conditions do not obtain, the mechanism probably produces a kind of continuum radiation or perhaps structured radiation more complex than the zebra bands.

In the case of our highly density-structured (ion-acoustic solitary) turbulent background plasma, transition radiation generated by the energetic electron component of a type IV burst should also contribute to the background and may in principle be responsible as well for providing waves at the upper hybrid frequency as a prerequisite to the zebra generation mechanism proposed.

We thank Gennady Chernov for illuminating discussions concerning his observations of the apparent sizes of zebras. We also thank Gregory Fleishman for pointing our attention to the importance of transition radiation. We are grateful to Barbara Mory and Brendan Cohen for technical support. The work of J. L. has been supported by NSF grant OPP-0090545 and NASA grant NAG 5-5318. The work by P. Y. was supported by NSF grant 0223764. R. T. thanks the International Space Science Institute Bern, where most of his work has been performed, for a senior visiting scientist fellowship, as well as for the hospitality of the ISSI staff.

APPENDIX A

For discrete modes to exist, we must have $Q^2(y) > 0$ at least for a finite range inside the region defined by $y < 1$, while $Q^2(y) < 0$ in the outer range $y > 1$. For this to happen, we must have $Q^2(y \to 1 + \epsilon) > 0$ and $Q^2(y > 1) < 0$; that is,

$$\frac{2}{\rho^2}\frac{1 + \alpha^2 + \delta\alpha^2 - x^2}{(1 + \delta)\alpha^2 x^2} - m^2 > 0, \qquad x^2 > 1 + \alpha^2 ,$$

or equivalently,

$$1 + \alpha^2 < x^2 < \frac{1 + \alpha^2 + \delta\alpha^2}{1 + (m^2\rho^2/2)(1 + \delta)\alpha^2} . \tag{A1}$$

However, for this relation to be meaningful, one must have

$$\frac{1 + \alpha^2 + \delta\alpha^2}{1 + (m^2\rho^2/2)(1 + \delta)\alpha^2} > 1 + \alpha^2 ,$$

which can be shown to reduce to

$$m^2 < \frac{2}{\rho^2}\frac{\delta}{(1 + \delta)(1 + \alpha^2)} . \tag{A2}$$

This shows that not all quantum numbers m are allowed, but only a few low-order numbers are meaningful.

As equation (A2) shows, the maximum quantum number ($m_{\max}$) is a function of the density enhancement δ and the plasma-to-cyclotron frequency ratio α. For moderate density enhancements $\delta \sim 1$ and moderate ratios α the denominator depends only weakly on these parameters, implying $m_{\max} \approx \sqrt{\delta}/\rho$, while for large $\delta \gg 1$, $m_{\max}$ becomes approximately independent of density. Since usually $\rho = \rho_e/L \ll 1$, the maximum azimuthal quantum number is thus essentially determined by the number of electron gyroradii fitting into the column. Existence of a small number of harmonics, resulting in few zebra stripes, might occur for narrow density enhancements (ρ small), small density enhancements (small δ), or large plasma-to-cyclotron frequency ratios (large α). This last condition is constrained by the double-resonance condition, so observations of few zebra stripes would more often correspond to one of the other two conditions; for example, narrow density enhancements result in small numbers of harmonics, and wide density enhancements result in large numbers of harmonics.

APPENDIX B

To analytically solve the integral in equation (10), define

$$q_\perp^2 \equiv \frac{2}{\rho^2}\frac{1 + (1 + \delta)\alpha^2 - x^2}{(1 + \delta)\alpha^2 x^2} .$$

Then we may write

$$I = \int_{y_*}^1 dy \sqrt{q_\perp^2 - \frac{m^2}{y^2}} = \int_{y_*}^1 dy \frac{\sqrt{q_\perp^2 y^2 - m^2}}{y} .$$

Let us further define

$$z^2 \equiv q_\perp^2 y^2 - m^2 .$$

Note that the lower bound of the z-integral is zero, since

$$q_\perp^2 y_*^2 - m^2 = 0 .$$

If we define

$$z_m \equiv \sqrt{q_\perp^2 - m^2} ,$$

then we may rewrite

$$I = \int_0^{z_m} \frac{z^2 dz}{z^2 + m^2} = z_m - m \arctan\frac{z_m}{m} ,$$

where the well-known integral indentity

$$\int \frac{dx}{x^2 + 1} = \arctan x$$

has been used. We then obtain the desired dispersion equation for the discrete eigenmodes

$$\zeta_m - \arctan\zeta_m = \frac{(2n + 1)\pi}{2m} ,$$

where

$$\zeta_m = \left[\frac{2}{m^2\rho^2}\frac{1+(1+\delta)\alpha^2-x^2}{(1+\delta)\alpha^2x^2}-1\right]^{1/2},$$

$n = 0, 1, 2, \ldots$ are arbitrary integers, and m is an integer greater than 1, subject to the constraints implied by equations (A1) and (A2).

REFERENCES

Bernold, T. 1980, A&AS, 42, 43
Chernov, G. P. 1990, Sol. Phys., 130, 75
———. 1996, Astron. Rep., 40, 561
Chernov, G. P., Markeev, A. K., Poquérusse, M., Bougeret, J. L., Klein, K.-L., Mann, G., Aurass, H., & Aschwanden, M. J. 1998, A&A, 334, 314
Chernov, G. P., Poquérusse, M., Bougeret, J. L., & Zlobec, P. 1999, in Magnetic Fields and Solar Processes, ed. A Wilson (ESA SP-448; Noordwijk: ESA), 765
Chiuderi, C., Giachetti, R., & Rosenberg, H. 1973, Sol. Phys., 33, 225
Davidson, R. C. 1972, Methods in Nonlinear Plasma Theory (New York: Academic Press), 20, 72
Etcheto, J., Christiansen, P. J., Gough, M. P., & Trotignon, J. G. 1982, Geophys. Res. Lett., 9, 1239
Fleishman, G. D. 2001, Astron. Lett., 27, 254
Fleishman, G. D., & Kahler, S. W. 1992, ApJ, 394, 688
Fleishman G. D., & Tokarev, Yu. V. 1995, A&A, 293, 565
Fomichev, V. V., & Fainshtein, S. M. 1981, Sol. Phys., 71, 385
Ginzburg, V. L., & Tsytovich, V. N. 1984, Transition Radiation and Transition Scattering (Moscow: Nauka; 1990, Bristol: Adam Hilger)
Gray, P. C., Hudson, M. K., Lotko, W., & Bergmann, R. 1991, Geophys. Res. Lett., 18, 1675
Horton, W., & Ichikawa, Y.-H. 1996, Chaos and Structures in Nonlinear Plasmas (Singapore: World Scientific), 165, 223
Jiřička, K., Karlicky, M., Meszarosova, H., & Snizek, V. 2001, A&A, 375, 243
Kuipers, J., van der Post, P., & Slottje, C. 1981, A&A, 103, 331
LaBelle, J., & Treumann, R. A. 2002, Space Sci. Rev., 101, 295
LaBelle, J., Trimpi, M. L., Brittain, R., & Weatherwax, A. T. 1995, J. Geophys. Res., 100, 21953
Ledenev, V. G., Karlicky, M., Yan, Y., & Fu, Q. 2001, Sol. Phys., 202, 71
Lee, J., Gallagher, P. T., Gary, D. E., Nita, G. M., Choe, G. S., Bong, S.-C., & Yun, H. S. 2003, ApJ, 585, 524
McAdams, K. L., Ergun, R. E., & LaBelle, J. 2000, Geophys. Res. Lett., 27, 321
Muschietti, L., Ergun, R. E., Roth, I., & Carlson, C. W. 1999, Geophys. Res. Lett., 26, 1093
Rosenberg, H. 1972, Sol. Phys., 25, 188
Shepherd, S. G., LaBelle, J., & Trimpi, M. L. 1998, J. Geophys. Res., 103, 2219
Slottje, C. 1972, Sol. Phys., 25, 210
———. 1981, Atlas of Fine Structures of Dynamics Spectra of Solar Type IV-dm and Some Type II Radio Bursts (Utrecht: Publ. Utrecht Obs.)
Treumann, R. A., & Bernold, T. E. X. 1981, Phys. Rev. Lett., 47, 1455
Treumann, R. A., Güdel, M., & Benz, A. O. 1990, A&A, 236, 242
Treumann, R. A., LaBelle, J., & Bauer, T. H. 1995, in Physics of the Magnetopause, ed. P. Song, B. U. Ö. Sonnerup, & M. F. Thomsen (Geophys. Monogr. 90; Washington: AGU), 331
Winglee, R. M., & Dulk, G. A. 1986, ApJ, 307, 808
Yoon, P. H., Weatherwax, A. T., & LaBelle, J. 2000, J. Geophys. Res., 105, 27589
Yoon, P. H., Weatherwax, A. T., & Rosenberg, T. J. 1998, J. Geophys. Res., 103, 4071
Zheleznyakov, V. V., & Zlotnik, E. Ya. 1975, Sol. Phys., 43, 431